

**Magnetic spring characteristic of an oscillatory actuator with silicone rubber torsion springs
for optical scanner applications**

Yinggang Bu^{a,*}, Hideyuki Kinjo^a, Kazuaki Oyaizu^a, Kaname Inoue^a, Tsutom Mizuno^a,
and Zhihui Duan^b,

^a Faculty of Engineering, Shinshu University, 4-17-1 Wakasato, Nagano, Japan

^b Optoelectronics Co., Ltd., 12-17-4, Tsukagoshi Warabi Saitama, Japan

Abstract: A compact electro-magnetic oscillatory actuator was proposed based on a pair of torsion springs for optical scanners operating at low oscillating frequencies, such as 50 Hz for a portable barcode scanner. Each torsion spring in the actuator is made of silicone rubber and is dually supported at both ends. A yoke is coupled with the driven coil to enhance the driving torque of the actuator. In this study, we analyzed the effect of the yoke on the resonant frequency of the actuator, as well as the torsion moment. We also experimentally determined the relationship between the resonant frequency and the magnetic gap of the yoke. Compared with the mechanical resonant frequency in the experiments, which was designed to be 50 Hz, the frequency was modified to 57.4 Hz, 54.7 Hz and 52.9 Hz when the gap between the yoke and the permanent magnet was 1.5 mm, 1.7 mm and 1.9 mm, respectively. The proposed actuator, which combines a

*Corresponding author. Tel.: +81 26 269 5181; Fax: +81 26 269 5215.
E-mail: buyinggang@shinshu-u.ac.jp (Y. Bu)

yoke with flexible torsion springs, is potentially useful as a compact optical scanner, taking advantages of both low power consumption and high reliability.

Keywords: optical scanner; oscillatory actuator; torsion spring; silicone rubber; magnetic spring.

1. Introduction

Optical scanners are widely used in applications, such as barcode readers and laser beam printers, in which single or multiple laser beams are used to scan printed patterns on objects. A handy terminal with an integrated optical scanner can rapidly enter the barcode information of articles by sweeping a laser beam across barcodes and can further assist in managing inventory in real time. With the rapid growth in the use of compact terminals, low power consumption and high reliability are strictly required for the optical scanners integrated in such terminal devices.

Typical optical scanners use polygon mirrors [1], MEMS (Micro Electro Mechanical Systems) mirrors or galvanic mirrors to realize high scanning performance. The most popular method is to use a polygon mirror because a wide scan angle is easily achieved simply by selecting the proper number of reflective surfaces. However, multiple reflective surfaces result in large mirror and driving motor sizes; thus, it is difficult to realize the merits of low power consumption and compact size at the same time. The MEMS technique used in semiconductor processing has used

in micro sensors and actuators[2,3], and this technique is an ideal method for developing thin optical scanners [4-9]. However, the use of piezoelectric or electrostatic elements to drive a MEMS scanner generally requires a high voltage in the electronic circuitry, which is difficult to achieve in low-cost portable devices [7-9]. Though several electro-magnetic techniques for driving MEMS scanners at relatively lower voltage have been developed, the open magnetic loop in these schemes requires a large permanent magnet located on the same plane of the scanner mirror; thus, it is hard to achieve a compact size [10-11]. In addition, portable devices must exhibit high reliability to unexpected shocks. Because MEMS scanners are generally manufactured using hard silicon materials, to achieve a low resonant scan rate, i.e., below 100Hz, the torsion spring must be very narrow such that it is weakly affected by such shocks in real applications if a delicate package design is not adopted.

In our previous research, a cantilever torsion spring composed of stainless steel was proposed to develop a compact optical scanner exhibiting low power consumption and high reliability [12]. In the structure, two stainless steel plates positioned orthogonal to each other were used to build the torsion spring. However, through the manufacture of a prototype, it was observed that high skill is necessary to assemble the steel plates; otherwise, it is difficult to achieve uniform performance in practical volume production.

In this paper, we propose a torsion actuator composed of a pair of torsion springs in which each spring has one end fixed to a support and the free ends of the springs are coupled to one another

by a center block. Both torsion springs are made of silicone rubber, which is expected to be an ideal material, rather than the stainless steel used to construct spring plates, because it is easy to mold into complex shapes at relatively low temperatures and retains good elastic strength at low frequencies. A permanent magnet is coupled to the center block and rotates around the torsion axis of the springs. The torsion springs, the center block and the magnet constitute the mover of the actuator. The stator of the actuator consists of a coil assembly and a yoke that face the magnet. The yoke is expected to enhance the torsion moment of the actuator; however, it also constantly produces a magnetic attraction force to the permanent magnet and pulls the mover towards the stator during torsion movement. In this study, the effect of the yoke was investigated. We analyzed the magnetic spring characteristics of the yoke using the finite element method (FEM) and experimentally evaluated the performance of the device thereafter using an actuator prototype. The relationship between the resonant frequency and the magnetic gap was experimentally determined.

2. Mechanical structure and principle

Fig. 1 illustrates the operating principle of a retro-reflective-type barcode scanner. A collimated laser beam generated by a semiconductor laser source first passes through the center hole of the collecting mirror and is then reflected by the scanning mirror toward the barcode plane. The scanning mirror is driven by an oscillatory actuator to sweep the outgoing laser beam across the

barcode. The backscattered light from the barcode is reflected by the same scanning mirror and is then guided to the photodiode by the collecting mirror. The collecting mirror features a concave reflective surface; thus, the backscattered light is concentrated on the photodiode, where the amplitude of the electric signal is representative of the physical state of the printed barcode.

2.1 Proposed structure

The basic structure of the proposed torsion actuator is shown in Fig. 2. Fig. 2 (a) shows a perspective illustration of the 3D model of the actuator. The mover of the actuator consists of the scanning mirror mentioned above, a permanent magnet, a pair of torsion springs and a center block coupled with both springs. The mirror is located on the front surface of the center block to sweep the incident laser beam, and the permanent magnet is located on the rear surface to generate the driving force. The pair of torsion springs are symmetrically coupled to the block at one end and connected to the support (not be shown) at the end. Compared with the torsion structure we previously developed, in which only one cantilever torsion spring was used, the symmetric dual springs will limit the vibration perpendicular to the torsion axis so as to effectively reduce unnecessary wobble disturbances affecting the scan line.

The center block is generally manufactured from a plastic material to achieve good adhesion to the scanning mirror and the magnet. However, the post-assembly process employed to connect such a small center block to the torsion springs requires the use of expensive assembly apparatus

and may introduce unexpected deformations into the torsion springs during the assembly process. To manufacture a sample prototype, we molded the center block and the torsion springs from the same silicone material, thus eliminating the delicate assembly process. The stator of the actuator is composed of a coil assembly, a yoke and the support mentioned above. The coil assembly consists of a bobbin with a hollow space along the x direction and a coil with 1100 turns. To achieve a high magnetic torque to drive the mover, a magnetizable yoke was inserted through the hollow space of the coil bobbin and positioned facing the permanent magnet. As illustrated, because the yoke and the permanent magnet generate an attractive magnetic force, the torsion springs will be constantly pulled towards the yoke. This force will change the gap between the springs slightly and result in a geometrical aberration relative to the initial mechanical design. To reduce this aberration, thicker torsion springs are preferred along the direction of this attractive force. As illustrated in the plane view of the pair of torsion springs in Fig. 2 (b), the cross-sectional dimensions of the springs were designed to be 1 mm along the x direction and 1.2 mm along the y direction. We will discuss this aberration produced by the attractive interaction between the yoke and the magnet in the following sections and further discuss its effect on the resonant frequency.

Fig. 2 (c) shows the top view of the proposed actuator. A square cubic neodymium magnet with dimensions of $L2 \text{ mm} \times W2 \text{ mm} \times D1.2 \text{ mm}$ faces the yoke. The yoke is composed of a soft magnetic steel material and measures $L8.2 \text{ mm} \times W2 \text{ mm} \times D0.5 \text{ mm}$. The air gap g is defined as the distance between the yoke and the magnet. When applying a current to the coil, a magnet force

along the x direction is induced in the magnet, and the torque moment of the torsion springs causes the mover to rotate around the z axis. The elastic energy in the torsion springs generates a restoring force that further induces oscillatory motion. In principle, any elastomer can be used to mold the torsion springs. Considering the wide operating temperature range required of portable optical scanners, a silicone elastomer (for example, XE20-500 series from Momentive Performance Materials LLC, KE-900 series from Shin-Etsu Chemical Co., Ltd.) was selected to produce the proposed actuator.

2.2 Oscillating mechanical model

The mechanical model of the proposed actuator is illustrated in Fig. 3. The movement function of the mover can be described by Eq. (1) :

$$J\ddot{\theta} + C\dot{\theta} + (K_m + K_s)\theta = T \quad (1)$$

where J is the moment of inertia of the mover, C is the damping constant, T is the torque of the actuator, K_m is the magnetic spring constant and K_s is the mechanical spring constant of the torsion springs.

Correspondingly, the oscillatory resonant frequency f_0 can be determined using Eq. (2) :

$$f_0 = \frac{1}{2\pi} \sqrt{\frac{K_m + K_s}{J}} \quad (\text{Hz}) \quad (2)$$

where J was calculated to be $1.46 \times 10^{-9} \text{ kg/m}^2$ using 3D modeling software.

2.3 Prototype actuator

Fig. 4 shows a photograph of the prototype actuator based on the proposed structure. We first molded the torsion springs and the center block structure with HCR (Heat Cured Rubber) silicone rubber (XE20-523-5U) at 180°C for 15 minutes and then cured the material at 200°C for 4 hours. We then bonded the ends of the torsion springs to a polycarbonate supporting plate using an adhesive (SUPER X LL No.8008) and adhered the mirror and the magnet to the opposite surfaces of the center block using the same adhesive. Finally, we heated the mover and the support in a temperature chamber for approximately 20 minutes to cure the adhesive. The yoke and the coil assembly in the stator were installed on a precision stage, making it convenient to adjust the air gap between the yoke and the magnet in the following experiments. The overall dimensions of the prototype actuator, including the stator, are approximately L10 mm×W10 mm×D10 mm. In a typical retro-reflective optical system, because a larger scanning mirror has the advantage of providing a higher signal intensity, a large scanning mirror with dimensions of L10 mm×W7 mm×D0.55 mm was used. The mirror was coated with a dielectric optical film on BK7 glass to improve the reflectance.

3 Characteristics of the magnetic spring

3.1 Mechanical spring constant

To determine the effect of the yoke, we first investigated the mechanical torque of the torsion springs. We released the yoke from the coil assembly and measured the torque of the torsion springs using a precise micro load cell. By increasing the rotating angle, the torsion torque was correspondingly increased. The relationship between the rotating angle and the measured elastic torque is shown in Fig. 5. The corresponding torsion spring constant K_s is calculated from the slope of the curve. Though the relationship is nonlinear when the rotating angle is greater than ± 10 degrees, we only used the linear section to estimate the torsion spring constant in the experiments; the resulting constant was estimated to be $K_s = 142.8 \mu\text{N}/\text{rad}$.

We then analyzed the magnetic spring constant by nonlinear static magnetic field analysis using FEM. The conditions of the analysis are shown in Table 1, and the simulated relationship between the magnetic torque and the rotating angle is illustrated in Fig. 6. The magnetic spring constant K_m was calculated from the slope of the curve. When only considering the linear region shown in Fig. 6, the magnetic spring constant was estimated to be $K_m = 42.6 \mu\text{N}/\text{rad}$, $27.3 \mu\text{N}/\text{rad}$ and $17.1 \mu\text{N}/\text{rad}$, when the air gap g was set to 1.5 mm, 1.7 mm and 1.9 mm, respectively. At a torsion spring constant of $K_s = 142.8 \mu\text{N}/\text{rad}$, it is clear that the magnetic spring constant will contribute

29.8%, 19.1% and 12.0% more to the oscillatory movement function corresponding to the different gap distances, respectively.

3.2 Influence of magnetic spring to the resonant frequency

We installed the yoke on the coil bobbin again and then experimentally investigated the effect of the yoke on the oscillatory characteristics of the device. As indicated by the FEM results, if the air gap g is 1.5 mm, 1.7 mm or 1.9 mm, the resonant frequency f_0 will drift from the original mechanical resonant frequency of 49.8 Hz to 56.7 Hz, 54.3 Hz or 52.7 Hz, respectively. To confirm these results, we experimentally investigated the effect on the actuator prototype. Fig. 7 shows a diagram of the rotation angle measurement. A collimated laser beam was incident to the scanning mirror at an angle of 45 degrees and reflected onto a screen located at a distance of $L_0=200$ mm. By tuning the applied sinusoidal driving signal with the frequency from 45 to 65 Hz, we plotted the relationship between the applied frequency and the oscillatory angle. The oscillatory angle can be calculated from the length of the scan line x and the screen distance L_0 . Fig. 8 shows a photograph of the experimental set-up.

Fig. 9 illustrates the effects of different gap distances on the behavior of the magnetic springs. Compared to the resonant frequency of 50 Hz without the yoke, the resonant frequencies are increased to 57.4 Hz, 54.7 Hz and 52.9 Hz when the gap distance is 1.5 mm, 1.7 mm and 1.9 mm. These results agree perfectly with the FEM results. In the experiments, to maintain a scanning angle of 60 degrees, the driving voltages with the yoke were 2.16 V (peak to valley level), 2.40 V

and 2.59 V, and the driving actual power were 4.49 mW, 5.54mW and 6.45 mW, respectively, corresponding to the abovementioned gaps. Compared with the voltage of 5.66 V and the power of 30.81mW without the yoke and an air gap $g= 1.7$ mm, the incorporation of the yoke significantly suppresses the power consumption.

Using the measured resonant frequency, the magnetic spring constant K_m can be derived from Eq. (2). The effect of the gap distance on the resonant frequency f_0 and magnetic spring constant K_m in the above experiments is illustrated in Fig. 10. At air gaps $g = 1.5$ mm, 1.7 mm, 1.9 mm, because the magnetic spring constant K_m was reduced to 47.1 $\mu\text{N}/\text{rad}$, 29.6 $\mu\text{N}/\text{rad}$ and 18.5 $\mu\text{N}/\text{rad}$, respectively, the resonant frequency of the actuator was reduced from 57.4 Hz to 52.9 Hz.

4. Magnetic flux distribution in the air gap

The typical distribution of the magnetic flux density under such gap distances was simulated using FEM. Fig. 11 (a) and Fig. 11 (b) show the simulated magnetic flux distribution when the air gap distance is 1.5 mm at different rotating angles. The figures demonstrate that the magnetic flux of the permanent magnet is nearly zero at the center of the yoke when the rotating angle is relatively small. We also simulated the magnetic flux distribution when the gap was changed to 1.9 mm. Although the magnetic flux density at the center is lower than that shown in Fig. 11, Fig. 12 shows that the flux from the permanent magnet is still zero around the center of the yoke. It is a

potential advantage for us that a relatively larger assembly tolerance is permitted in volume production.

5. Conclusions

In this study, we designed a torsion actuator composed of a pair of silicone rubber torsion springs to develop a low-resonant-frequency optical scanner and manufactured an actuator prototype to demonstrate the feasibility of the scanner. The effect of the yoke was investigated by both FEM calculations and experiments. Because the magnetic spring from the yoke will change the resonant frequency and is dependent on the gap distance from the permanent magnet, the results reported in this paper should provide valuable design information to optimize the actuator's overall performance in a practical portable optical scanner. In addition, by manufacturing the actuator prototype using silicone rubber, we demonstrated the feasibility of the volume production of such an elastomer torsion spring.

6. References

[1] T. Ohji, S. Ikeno, K. Amei, M. Sakui and S. Yamada, Development of a polygon scanner motor using single-axis controlled repulsive type magnetic bearing system, *International Journal of Applied Electromagnetics and Mechanics* **19** (2004) 139–144.

- [2] H. Cao and H. Li, Investigation of a vacuum packaged MEMS gyroscope architecture's temperature robustness, *International Journal of Applied Electromagnetics and Mechanics* **41** (2013) 495-506.
- [3] T. Creutzburg, L. Rissing, T. Lenarz, G. Reuter, Design and fabrication of a microactuator for a hearing aid, *International Journal of Applied Electromagnetics and Mechanics* **39** (2012) 471-477.
- [4] N. Asada, H. Matsuki, K. Minami and M. Esashi, Silicon micromachined two-dimensional galvano optical scanner, *IEEE Transactions on Magnetics* **30** (1994), 4647-49.
- [5] S. Eliahou-Niv, Design, analysis and fabrication of a new MEMS scanning device actuator, *Applied Surface Science* **248** (2005), 503-08.
- [6] Y. M. Liu, J. Xu, S. L. Zhong and Y. M. Wu, Large size MEMS scanning mirror with vertical comb drive for tunable optical filter, *Optics and Lasers in Engineering* **51** (2013), 54-60.
- [7] S. H. Xiang, S. H. Chen, X. Wu, D. Xiao and X. W. Zheng, Study on fast linear scanning for a new laser scanner, *Optics and Laser Technology* **42** (2010), 42-46.
- [8] Y. Du, G. Zhou, K. K. L. Cheo, Q. Zhang, H. Feng, B. Yang and F. S. Chau, High speed laser scanning using MEMS driven in-plane vibratory grating: design, modeling and fabrication, *Sensors and Actuators A: Physical* **156** (2009), 134-44.

- [9] Y. C. Ko, J. W. Cho, Y. K. Mun, H. G. Jeong, W. K. Choi, J. W. Kim, Y. H. Park, J. B. Yoo, and J. H. Lee, Eye-type scanning mirror with dual vertical combs for laser display, *Sensors and Actuators A: Physical* **126** (2006), 218-26.
- [10] L. O. S. Ferreira and S. Moehlecke, A silicon micromechanical galvanometric scanner, *Sensors and Actuators a-Physical* **73** (1999), 252-60.
- [11] T. Fujita, K. Maenaka, and Y. Takayama, Dual-axis MEMS mirror for large deflection-angle using su-8 soft torsion beam, *Sensors and Actuators A: Physical* **121** (2005), 16-21.
- [12] T. Mizuno, Y. Hattori, Y. Bu, R. Aotsuka and Y. Teramae, Consideration on linear oscillatory actuator for optical Scanner, *The 7th International Symposium on Linear Drives for Industry Applications* **OS9.1** (2009), 156-57.

Caption of all figures:

Fig. 1. The operating principle of a retro-reflective-type barcode scanner.

Fig. 2. Basic structure of the oscillatory actuator : (a) 3D model of the structure (b) the dimension of the silicone rubber torsion springs (c) Top view of the structure (unit: mm).

Fig. 3. Mechanical model of proposed actuator.

Fig. 4. Photograph of the prototype actuator.

Fig. 5. Mechanical torque of the torsion spring vs. rotation angle.

Fig. 6. Magnetic torque vs. rotation angle.

Fig. 7. Diagram of rotation angle measurement.

Fig. 8. Photograph of rotation angle measurement set-up.

Fig. 9. Scanning angle vs. resonant frequency.

Fig. 10. Resonant frequency and magnetic spring constant as a function of the air gap distance.

Fig. 11. Magnetic flux distribution at $g = 1.5$ mm : (a) $\theta = 0$ deg. (b) $\theta = 15$ deg..

Fig. 12. Magnetic flux distribution at $g = 1.9$ mm : (a) $\theta = 0$ deg. (b) $\theta = 15$ deg..

Figures

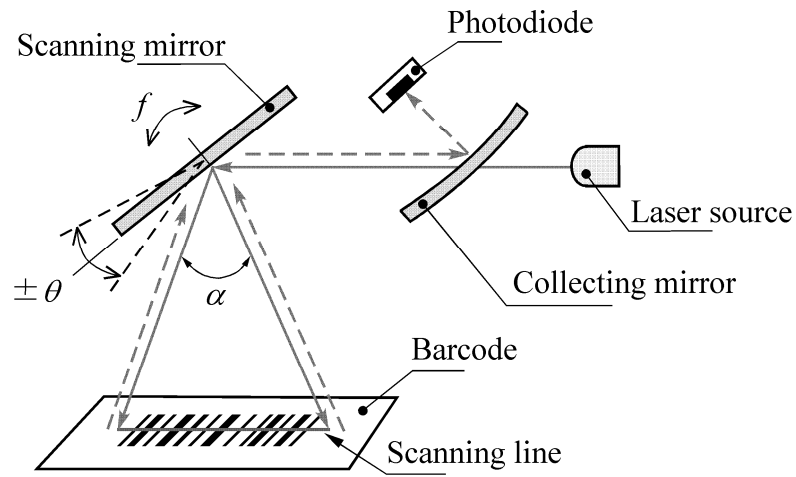


Fig. 1. The operating principle of a retro-reflective-type barcode scanner.

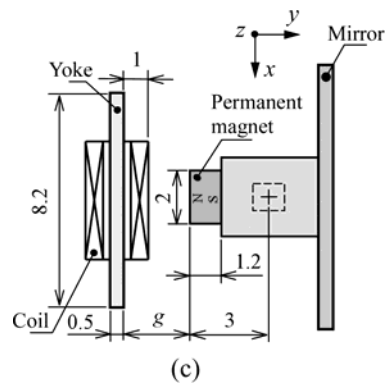
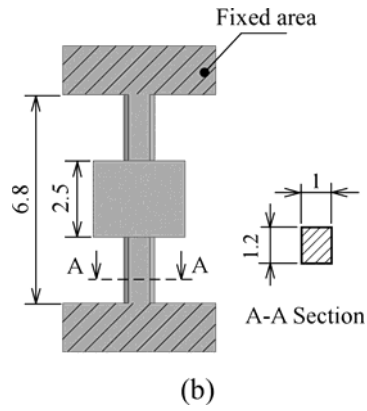
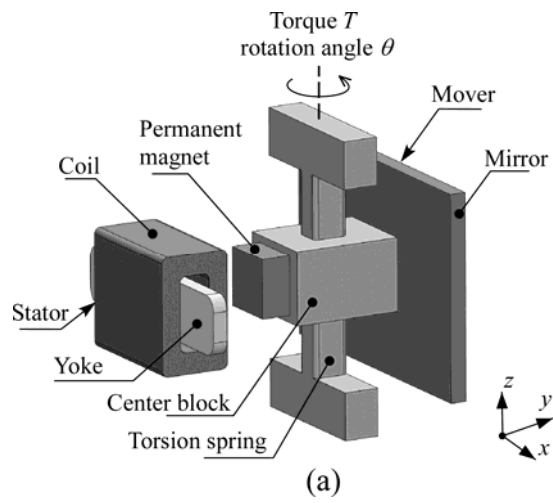


Fig. 2. Basic structure of the oscillatory actuator : (a) 3D model of the structure (b) the dimension of the silicone rubber torsion springs (c) Top view of the structure (unit: mm).

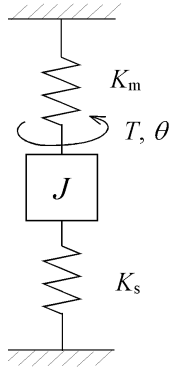


Fig. 3. Mechanical model of proposed actuator.

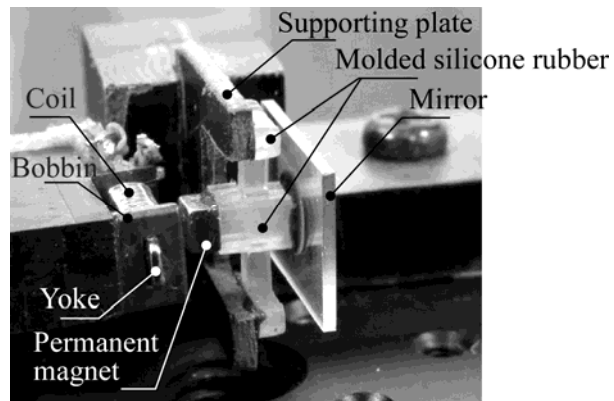


Fig. 4. Photograph of the prototype actuator.

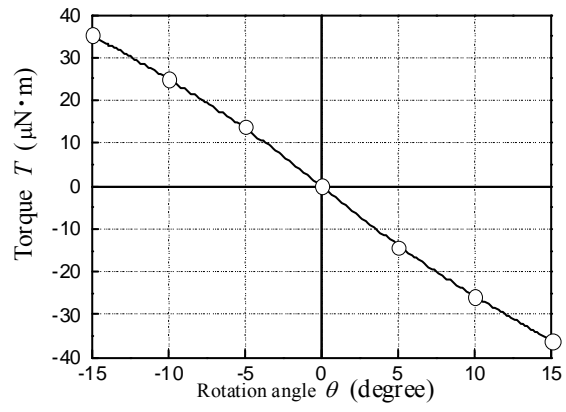


Fig. 5. Mechanical torque of the torsion spring vs. rotation angle.

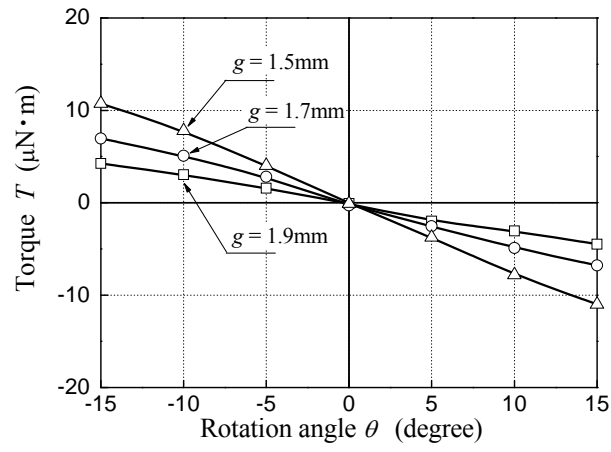


Fig. 6. Magnetic torque vs. rotation angle.

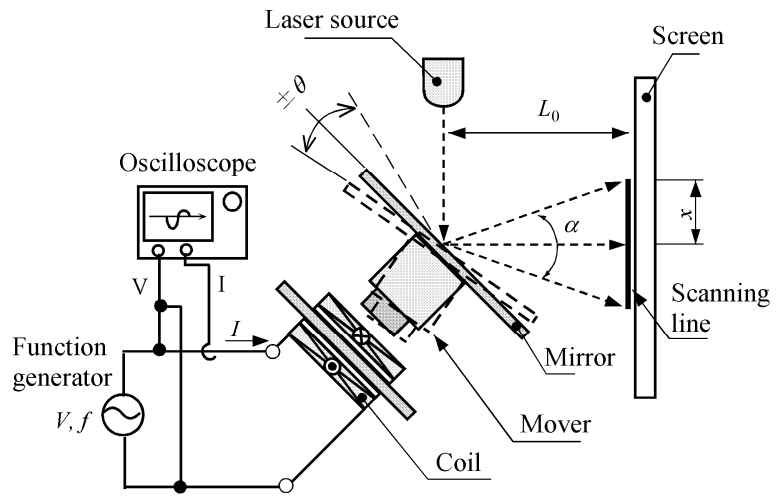


Fig. 7. Diagram of rotation angle measurement.

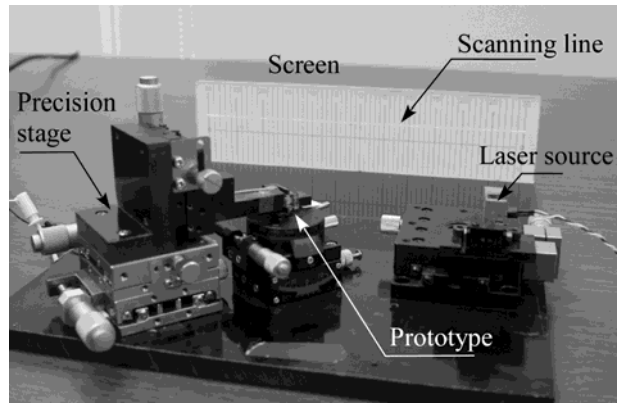


Fig. 8. Photograph of rotation angle measurement set-up.

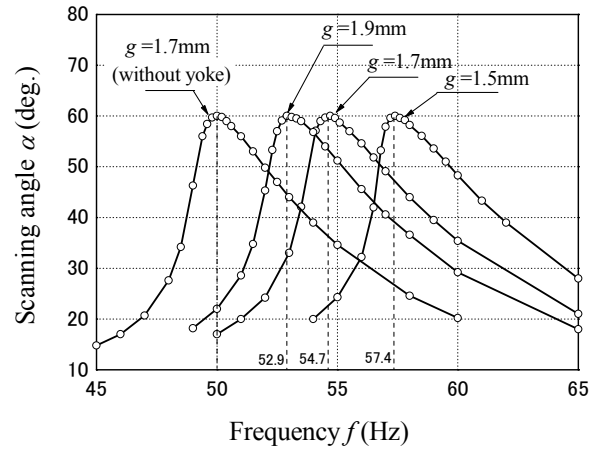


Fig. 9. Scanning angle vs. resonant frequency.

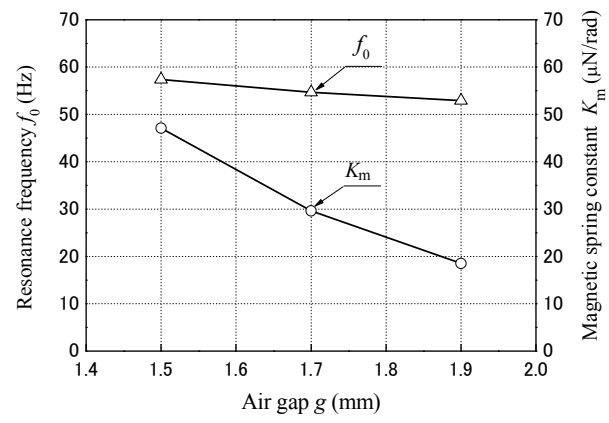


Fig. 10. Resonant frequency and magnetic spring constant as a function of the air gap distance.

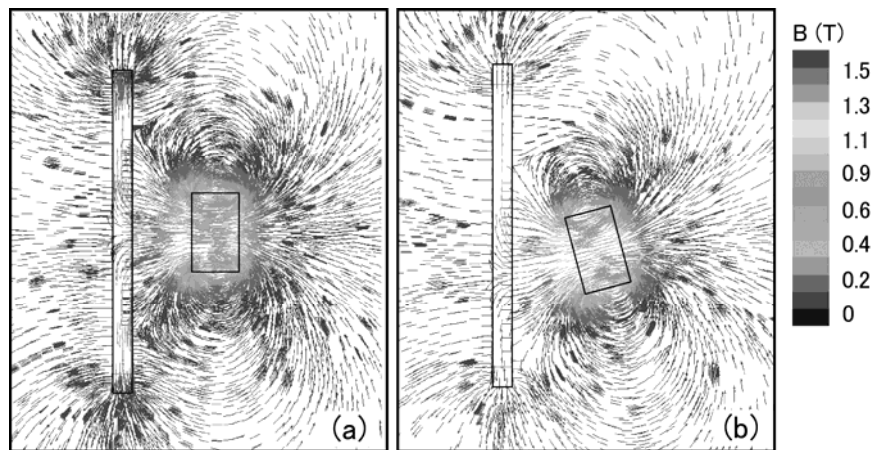


Fig. 11. Magnetic flux distribution at $g = 1.5$ mm : (a) $\theta = 0$ deg. (b) $\theta = 15$ deg..

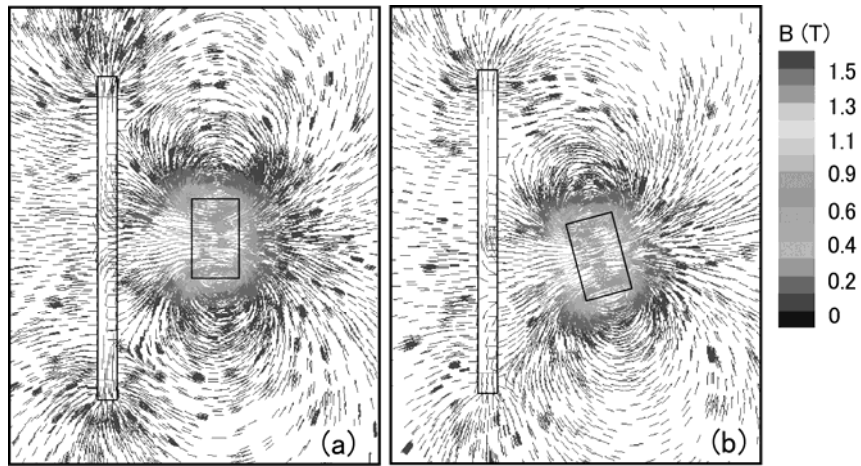


Fig. 12. Magnetic flux distribution at $g = 1.9$ mm : (a) $\theta = 0$ deg. (b) $\theta = 15$ deg..

Table 1 Magnetic analysis conditions.

Item		Value	(unit)
Permanent magnet	Residual magnetic flux density	1.36	(T)
	Coercive force	1018	(kA/m)
	Maximum energy product	358	(kJ/m ³)
	Recoil permeability	1.06	
Air	Relative permeability	1	
Coil	Relative permeability	1	
Yoke	Saturation flux density	1.9	(T)
		(at $H = 15$ kA/m)	